


*Research Article*

Bidirectional Puc Converter Based Battery Storage System for Active and Reactive Power Control

Ahmet Mete VURAL ^{a,*} 

^a Electrical and Electronics Engineering, Faculty of Engineering, Gaziantep University, Gaziantep, Türkiye

ARTICLE INFO

Article history:

Received 12 September 2025
Accepted 20 October 2025

Keywords:

Battery storage system,
packed U-cell converter,
grid-tied mode,
stand-alone mode,
capacitor voltage control,
power control

ABSTRACT

Battery storage systems (BSS) play a crucial role in enhancing power quality, reliability, and renewable energy integration. However, multilevel converters used in BSS often face challenges of high component count and capacitor voltage balancing. This study addresses these issues by proposing a single-phase battery storage system based on a seven-level packed U-cell (PUC) converter with two DC-links. Each DC-link is regulated by a bidirectional DC-DC converter, ensuring stable capacitor voltage control and enabling seamless operation in both grid-tied and stand-alone modes under a unified control scheme. Unlike conventional approaches that redesign controllers for different modes, the proposed system only modifies the reference voltage generation for pulse-width modulation. Simulation results confirm effective capacitor voltage balancing, smooth bidirectional active power transfer, and reliable reactive power exchange, allowing the BSS to function as a single-phase STATCOM. Harmonic analysis demonstrates compliance with IEEE 519–2014 standards, ensuring high power quality in grid-tied and stand-alone operation.

This is an open access article under the CC BY-SA 4.0 license.
(<https://creativecommons.org/licenses/by-sa/4.0/>)

1. Introduction

While fossil fuels have undeniably improved our lifestyles, their use has come at a significant environmental cost. Greenhouse gas emissions, primarily from CO₂, are accelerating global warming. Buildings are significant contributors, accounting for about 40% of global energy consumption and 36% of CO₂ emissions [1]. As energy demand and emissions continue to rise, there is an urgent need for solutions. Net-zero energy homes, which produce as much energy as they consume, offer a promising approach to reducing both energy use and greenhouse gases. On the other hand, energy storage offers both economic and environmental benefits. By optimizing storage and consumption, emissions resulting from traditional fossil fuel power plants can be significantly reduced [2], [3]. Battery storage systems (BSSs) are extensively used in electric vehicles, microgrids, renewable energy storage, household appliances, and more [4], [5]. BSSs also play a crucial role in energy arbitrage

by capitalizing on fluctuations in daily energy prices [6]. They enable the purchase of low-cost energy during periods of low demand, which is then stored in batteries. This stored energy can be utilized during peak demand when prices are higher [7]. Moreover, during a power outage, a BSS can supply loads for a limited period of time. Household-level battery storage is now emerging as the next generation of energy technology on the cusp of mass-market penetration [8], [9]. Small-scale BSS, particularly in behind-the-meter applications, can provide an effective solution for enhancing a home's resilience to power outages caused by storms, as demonstrated in [10]. In this study, a packed U-cell converter (PUC)-based single-phase BSS (PUC-BSS) is designed for low-power home applications. The designed BSS can operate either in grid-tied mode (charging or discharging the batteries) or in stand-alone mode (supplying the local load). PUC-BSS can also function as a single-phase STATCOM to exchange reactive power with the grid in two directions.

* Corresponding author. E-mail address: mvural@gantep.edu.tr
DOI: 10.58190/ijamec.2025.146

The combination of PUC units was used in a multilevel converter topology for the first time by researchers [11], [12]. The so-called PUC multilevel converter unifies the cascaded H-bridge (CHB) topology and flying capacitor (FC) topology. In this way, unlike other well-known converter topologies, such as neutral-point clamped (NPC), CHB and FC, the PUC multilevel converter requires the fewest number of power switches and capacitors for generating the same output voltage levels [12]. This advantage reduces the design cost and system complexity. Furthermore, conventional multilevel converters can have significant drawbacks as the number of voltage levels increases. Specifically, to generate five or more voltage levels, the number of switches, diodes, and capacitors increases substantially, leading to higher costs and making their implementation much more complex. However, the PUC multilevel converter has a modular assembly where many PUCs are connected to obtain the desired number of voltage levels with reduced stress on power semiconductors. Although the PUC topology has many advantages, unlike conventional two-level voltage source converter, PUC converter requires floating capacitor voltage balancing and control, which becomes a challenging goal as voltage level count increases. In the literature, generally closed-loop PI control or model predictive control (MPC) techniques are employed for capacitor voltage balancing/regulation in PUC converters. In [13], the grid current is utilized to balance the capacitor voltages for a single-phase PUC5 converter as an SVC. The system can inject or absorb reactive power to/from the grid. The proposed approach takes advantage of the redundant switches available in 5-level operation. In [14], capacitor voltage balancing is achieved for a PUC9 inverter that has three floating capacitors using the suggested modulation technique, eliminating the need for extra sensors to maintain capacitor voltage balance. An MPC approach is utilized for a single-phase active power filter employing a PUC5 converter to mitigate harmonic currents at the point of common coupling caused by nonlinear loads [15]. The results demonstrate that the DC-link voltage is effectively regulated, achieving a good balance between the two DC-link capacitor voltages. In [16], MPC is activated to regulate capacitor voltages of a multi-cell modular multilevel converter with a PUC structure for AC-AC and AC-DC applications. The study presented in [17] introduces a seven-level PUC based solar inverter with one DC source and two floating capacitors in its topology. The capacitor voltage is balanced in open-loop by applying a multi-carrier PWM technique. The study presented in [18] aims to design an advanced control method for a single-phase nine-level Packed E-Cell inverter used in stand-alone renewable energy systems. The proposed approach focuses on maintaining stable and balanced DC-link capacitor voltages while delivering accurate output voltage control with lower computational

effort than traditional predictive controllers. In [19], an MPC approach for PUC inverter is suggested to improve dynamic performance in microgrid applications. MPC focuses on achieving balanced capacitor voltages, improved power quality, and fast dynamic response under various operating conditions. A 5-level PUC-based active front-end rectifier is proposed and experimentally validated in [20] to effectively regulate the auxiliary capacitor voltage with a low-distorted voltage waveform at the output. Voltage Balancing is achieved by utilizing redundant switching states with a PI-controller structure. In this study, the voltage control for each capacitor of the PUC converter is achieved in a different way through DC-DC converters. Each DC-link capacitor voltage is controlled with a PI-control scheme that also regulates the current of each battery group. Although the PUC topology is implemented for solar PV [21]-[24], wind [25], SVC [13], active filter [15], [26], [27], STATCOM [28], [29], active front-end rectifier [20], and electric vehicle charging [30] applications, its usage in BSS applications is not common in practice [31]. In terms of BSSs, mostly conventional multilevel converters such as CHB and MMC topologies are employed [32]. Upon reviewing the literature, a three-phase BSS application utilizing a seven-level PUC converter is presented in [33]. The system employs a finite-set MPC approach to achieve satisfactory dynamic performance. However, this topology incorporates a single flying capacitor, whose voltage is regulated, and the upper DC-link is connected to a battery.

The operation of a solar PV system with storage is assessed using the seven-level PUC inverter interacting with zeta converter which controls the output voltage of the PV array, utilizing the MPPT algorithm [34]. However, battery charging is not considered and the system operates in only stand-alone mode without a STATCOM function. In [35], a grid-tied PUC converter employs MPC. One DC link of the PUC converter is connected to multiple batteries, and the power sharing among the batteries is managed using the droop control method. The other capacitor remains floating, and its voltage is regulated via MPC. Table 1 summarizes a recent comparison between this study and other PUC converter applications in the literature.

Table 1. Recent PUC Converter-Based Studies

Ref.	Control approach	Connection type	STATCOM function	Battery connection	Year
[14]	V/Hz control	Stand-alone	No	One DC-link	2024
[15]	MPC	Grid-tied	No	No	2020
[17]	V/Hz control	Stand-alone	No	One DC-link	2022
[19]	MPC	Grid-tied	Yes	No	2022
[20]	PI control	Grid-tied	Yes	No	2025
[21]	PI control	Grid-tied	Yes	No	2023
[22]	MPC	Grid-tied	Yes	No	2025
[23]	finite-set MPC	Grid-tied	Yes	No	2025
[24]	MPC	Grid-tied	Yes	No	2024
[25]	PI control	Stand-alone	No	No	2023
[26]	PI control and fuzzy logic	Grid-tied	No	No	2022
[28]	3 rd harmonic control	Grid-tied	Yes	No	2020
[30]	MPC	Grid-tied	No	No	2023
[33]	MPC	Grid-tied	Yes	One DC-link	2021
[34]	PI control	Stand-alone	No	One DC-link	2019
[35]	MPC	Grid-tied	No	One DC-link	2016
[36]	Fuzzy logic	Stand-alone	No	No	2023
[37]	Fuzzy logic	Stand-alone	No	No	2024
[38]	PID control	Grid-tied	No	One DC-link (only discharge)	2025
This study	PI control	Grid-tied and stand-alone	Yes	Two DC-links	

In this study, the active and reactive power outputs of the PUC converter is controlled in two directions in grid-tied mode. These enables the charging and discharging of the batteries and also makes reactive power control possible both in inductive and capacitive modes, like a STATCOM. The contributions of this study are;

To the best of the author's knowledge, for each DC-link of the PUC topology, a battery and a bidirectional DC-DC converter are used for the first time in a grid-tied battery storage application. The developed PUC-BSS is also used for stand-alone application (supplying a load).

While charging and discharging the batteries, the PUC-BSS can also function as a STATCOM, exchanging controlled reactive power with the grid in two directions.

A single control approach is used for regulating the capacitor voltages of the PUC converter operating both in

grid-tied and stand-alone modes. This control approach is based on the control of the bidirectional DC-DC converters connected to the batteries.

The remainder of this paper is organized as follows: Section 2 presents the circuit structure of the designed PUC-BSS, including the design stages of some electrical parameters. Section 3 summarizes the operation principle of the PUC converter, including its interaction with battery storage from DC-links. In Section 4, the control system for each power electronic interface in PUC-BSS is described using block diagrams. Section 5 presents and discusses the results of the simulated system under different operating modes. Finally, conclusion is given in Section 6.

2. THE CIRCUIT STRUCTURE OF PUC-BSS

The single-phase PUC-BSS circuit structure is given in Figure 1. By using the switches $sw1$ and $sw2$, the system can be connected to either the grid or the load in an isolated manner. A series L-filter L_f connects the PUC converter output to the grid. The DC-links of the PUC converter are fed from two bidirectional DC-DC converters, which are supplied from two battery groups. The system allows bidirectional active power flow such that the batteries can be either charged or discharged in grid-tied mode while the reactive power injected into the grid can be bidirectionally controlled. In this study, the 1700V-600A dual IGBT module FF600R17ME4 from Infineon is utilized as the switching element in the PUC converter [39]. This IGBT has a rated collector-emitter voltage of $V_{CES}=1200\text{ V}$ and a nominal continuous collector current rating of $I_C=600\text{ A}$. On the other hand, the semiconductor element for each DC-DC converter is a fast-switching MOSFET. Since the PUC converter is a voltage-sourced one, it should be fed from two DC voltages. To operate this converter stably, these DC voltages should be regulated at their references by a control system which is mentioned later. The reference voltages $E_{1,2(ref)}$ for the two DC-links of the PUC converter should be designed according to the following constraints;

$$\begin{cases} E_{1(ref)} \geq \frac{2}{m} \sqrt{\left(\frac{2}{3}\right) V_G} \\ E_{2(ref)} = \frac{1}{3} E_{1(ref)} \end{cases} \quad (1)$$

where, m is the modulation index of the PWM switching algorithm and V_G is the grid rms voltage. In this regard, $E_{1(ref)}$ and $E_{2(ref)}$ can be designed as 675 volts and 225 volts, respectively for a grid voltage of $V_G = 300\text{ V}$ and $m = 1$.

Since this study is based on a single-phase power system, a home application is a good example for this purpose. The capacity for each battery group can be

designed as $C_{ap1,2} = 150 \text{ Ah}$. The rated voltage of each battery group is specified as $V_{bat1} = 675 \text{ V}$ and $V_{bat2} = 225 \text{ V}$, respectively. To reach these voltages, different battery types and connection possibilities exist. For instance, for the battery group-1, 14 units of 48V-150Ah Li-ion or LiFePO4 batteries (connected in series) can be selected for their inherent advantages. Similarly, to reach the required voltage for the battery group-2, 5 units of 48V-150Ah batteries can be connected in series. The total capacity of the PUC-BSS can then be calculated as follows:

$$W_T = (C_{ap1})(V_{bat1}) + (C_{ap2})(V_{bat2}) = 135 \text{ kWh} \quad (2)$$

Although these capacities are not mandatory, this full capacity can sufficiently power three homes with four-people during one-day outage if each person is assumed to consume 10 kWh/day on average. In the simulation platform, aggregated battery model is preferred because of the purpose of the study. This means that a single generic Li-ion battery model is used to represent the multiple battery units connected in series. Since the observation of the voltage/current and SOC of each unit is not the aim of this study, this approach is sufficient to run the simulations. In the battery simulation block, basic

parameters such as nominal voltage, rated capacity, initial SOC, and battery response time can be defined as shown in Table 2. The effects of temperature and aging are ignored. The discharge characteristics are determined from the nominal battery parameters. In order to effectively observe the fast dynamics of voltage and current of each battery group, a relatively short response time of 1 second is chosen in the simulations. The battery is modeled using an equivalent circuit representation that accounts for both steady-state and dynamic behaviors [40]. This model includes an internal resistance and a controlled voltage source to represent the instantaneous voltage response. The open-circuit voltage is obtained from empirical functions of current and other battery parameters. To capture the transient voltage dynamics, a first-order relaxation effect typically observed in lithium-ion cells. A first-order low-pass filter is applied to smooth the current input. The SOC is continuously evaluated by integrating the input current over time. Finally, the terminal voltage of the battery is the sum of the open-circuit voltage, exponential voltage component, and the voltage drop across the internal resistance.

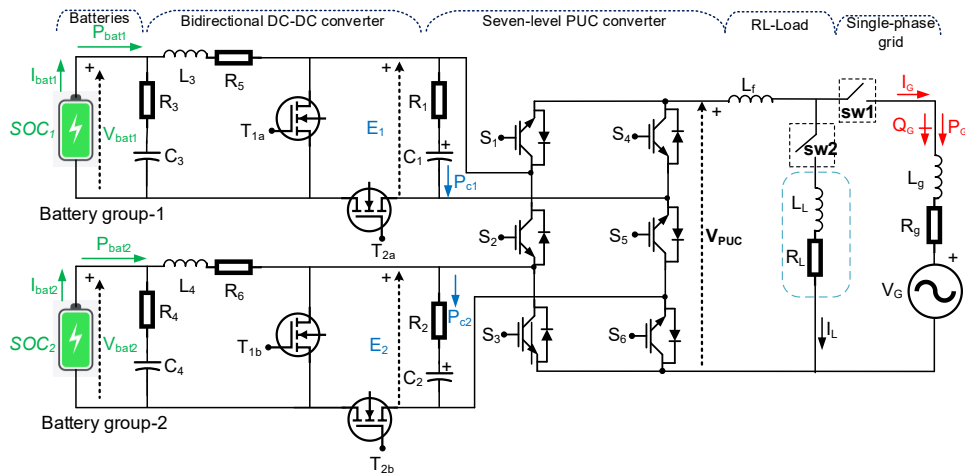


Figure 1. The Circuit Structure of Single-phase PUC-BSS

Table 2. The Simulation Parameters for Battery Groups

Battery Group-1 (14 units of Li-ion battery)	
Nominal Voltage	675V (14x48V)
Rated Capacity	150Ah
Initial SOC	50%
Response Time	1 s
Battery Group-2 (5 units of Li-ion battery)	
Nominal Voltage	225V (5x48V)
Rated Capacity	150Ah
Initial SOC	50%
Response Time	1 s

3. OPERATING PRINCIPLE OF PUC CONVERTER

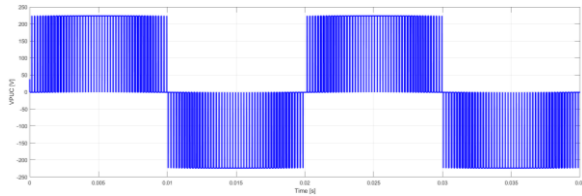
The PUC converter utilized in this study can generate a seven-level voltage output at the maximum modulation index. In the literature it is also called as the “PUC7”

converter. As shown in Figure 1, its power circuit consists of six power semiconductor switches, such as IGBTs and two isolated DC sources. The switch in each row operates in a complementary manner. One interesting feature of this topology is that depending on the voltage ratio ($\frac{E_1}{E_2}$), the output voltage level can be altered. If this ratio is 2, five-levels can be produced. If this ratio is 3, seven-levels can be attained at converter output. The cost advantage of the PUC converter compared with common multilevel converter topologies is shown in Table 3. As presented, it needs the fewest number of components to generate the same voltage level. However, its PWM switching scheme is not straightforward like those for NPC or CHB converters. The PUC converter requires a switching logic

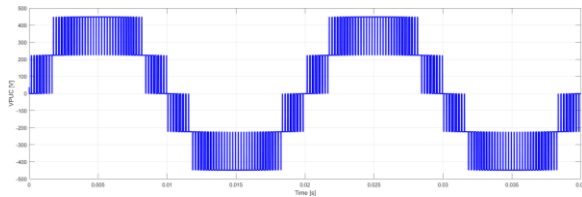
based on the necessary switching states to generate a multilevel staircase voltage waveform. In this study, a level-shifted PWM scheme is designed and will be discussed later. Figure 2 illustrates the output voltage waveforms of the PUC7 converter at no load under different modulation indices, with a PWM carrier frequency of 5 kHz and fundamental frequency of 50 Hz. As shown, the voltage level count depends on the modulation index and the maximum voltage level count is obtained when it is set to 1.

Table 3. Component Count Comparison of Some Seven-level Converter Topologies

Topology name	IGBT count	Capacitor count	Clamping diode count
NPC converter	24	6	20
CHB converter	12	3	0
PUC converter	6	2	0



(a) Modulation index $m = 0.33$



(b) Modulation index $m = 0.66$

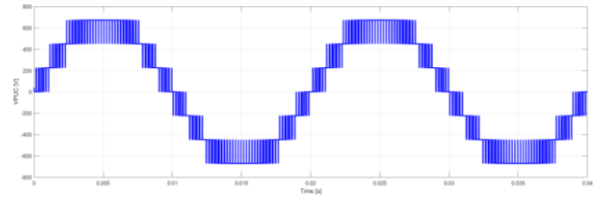
Table 4. The Status of the Batteries of the PUC Converter without Control

Battery-1 status	Battery-2 status	State number	Battery-1 status	Battery-2 status	State number
charge	-	1	-	-	5
charge	discharge	2	-	discharge	6
-	charge	3	discharge	charge	7
-	-	4	discharge	-	8

4. CONTROL SYSTEM DESIGN

The BSS control system consists of PUC converter control and DC-DC converter control. For grid-tied mode of operation, single-phase dq coordinate transformation of the grid voltage V_G and grid current I_G is needed to separately control active and reactive power injections from the BSS to the grid or vice versa. This transformation is realized using two cascaded first-order low-pass filters, as shown in Figure 3. The transfer function of the first-order low-pass filter is given by:

$$H(s) = \frac{1}{1+\tau s} \quad (3)$$



(c) Modulation index $m = 1.0$

Figure 2. The Output Voltage Waveform of the PUC7 Converter At No Load

According to the switching states of the PUC converter, the status of the batteries connected at the two DC-links are given in Table 4 without applying any charging/discharging control scheme. As shown, none of the battery states can be the same at any switching state. When one battery is charging, the other one is either discharging or in a no-action state. This means that with a direct battery connection to the DC-links of the PUC converter, it cannot function properly as a BSS, since the main aim of the BSS is that all the batteries in the system should charge or discharge in unison when required. This necessitates a control system for the proper charging and discharging events of the BSS. In this study, such a control system is designed and will be discussed in Section 4. The control principle involves replacing capacitors at the DC-links of the PUC converter and controlling their voltages using bidirectional DC-DC converters and batteries.

where $\tau = \frac{1}{2\pi f}$ is the time constant of the filter and f is the grid fundamental frequency. The frequency response of the first-order lowpass filter is illustrated in Figure 4. As shown, for $f = 50 \text{ Hz}$, the phase is shifted by 45° degrees and the magnitude is reduced by a factor of $\frac{1}{\sqrt{2}}$. If two such cascaded filters are connected to each other, the total phase shift of the input signal will be 90° degrees to obtain the *beta* component. Since the magnitude is reduced by a factor of 0.5, the output of the second filter is multiplied by 2 to compensate for the magnitude reduction. On the other hand, since the *alfa* component is equal to the input signal itself, it can be directly obtained without any filtering. Once the *alfa* and *beta* components are obtained,

the dq components are generated using *alfabeta-to-dq* transformation. In grid-tied mode, a single-phase phase-locked loop (PLL) is employed to align the BSS current with the phase and frequency of the grid voltage, ensuring proper control of active and reactive power injections from the BSS to the grid or vice versa. To obtain dq components of the grid voltage and the grid current, the synchronization signal wt is sent to *alfabeta-to-dq* transformation blocks as shown in Figure 3.

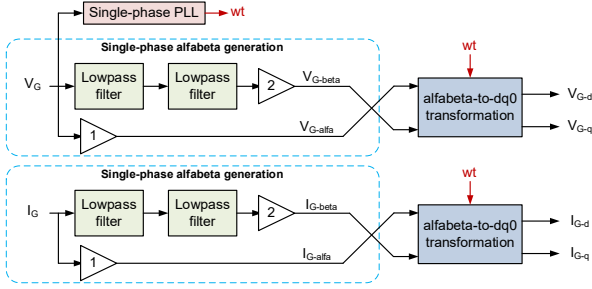


Figure 3. Single-phase dq Transformation

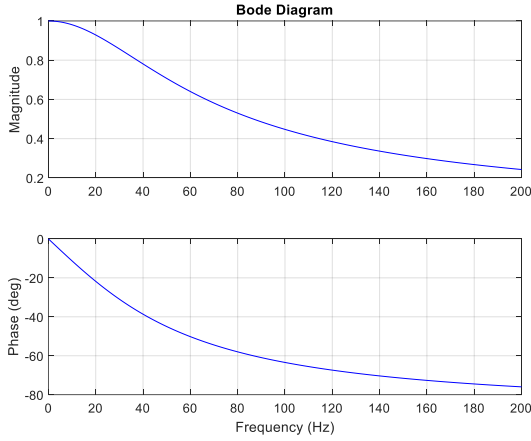


Figure 4. The Frequency Response of the First-order Lowpass Filter

4.1. PUC Converter Control

The PUC converter control scheme is shown in Figure 5. Depending on the operating mode, the reference voltage calculation for multi-carrier PWM generation is realized either by decoupled dq current control for grid-tied mode, or open-loop reference voltage generation for stand-alone mode. If the stand-alone mode is selected, the modulation index and the phase shift are entered manually. On the other hand, when the grid-tied mode is selected, the reference values for dq components of I_G are determined according to the functional requirements given in Table 5. According to this table, one can see that the PUC-BSS can

function as a STATCOM providing capacitive or inductive reactive power to the grid in grid-tied mode while the batteries can be either charged or discharged.

Table 5. Determination of the Reference Values for I_G dq Components in Grid-tied Mode

d -axis component	q -axis component (for STATCOM function)
$I_{G-d(ref)} < 0$ for charging the batteries (absorbing active power from the grid)	$I_{G-q(ref)} < 0$ for supplying reactive power to the grid (capacitive mode)
$I_{G-d(ref)} > 0$ for discharging the batteries (injecting active power to the grid)	$I_{G-q(ref)} > 0$ for absorbing reactive power from the grid (inductive mode)

In Figure 5, the reference and the measured values of d and q -axis current components are individually compared and sent to PI controllers. The decoupling gain $K_C = 2\pi f L_G$ is used to decouple the cross-coupling terms by adding compensating terms with opposite signs. This enables the controller to manage both the magnitude and phase of the output current independently, which is crucial for regulating the active and reactive power injections P_G and Q_G from the BSS to the grid, expressed as below:

$$\begin{cases} P_G = \frac{1}{2}(V_{G-q}I_{G-q} + V_{G-d}I_{G-d}) \\ Q_G = \frac{1}{2}(V_{G-q}I_{G-d} - V_{G-d}I_{G-q}) \end{cases} \quad (4)$$

The $dq0$ -to-*alfabeta* transformation block generates $V_{PUC-alfa}$, which is multiplied by $\frac{1}{E_1}$ to extract the reference voltage waveform $V_{PUC(ref)}$ for level-shifted PWM generation to produce the switching signals for the PUC converter. In this study, phase disposition PWM (PD-PWM), one of the level-shifted PWM methods, is preferred over phase-shifting PWM due to its low switching losses [41]. Figure 6. shows the reference and carrier waveform instants for PD-PWM in stand-alone operation. As shown, all the carrier signals are aligned in phase but positioned at different levels. This implies that the carriers are shifted vertically without any phase shift. When the carriers are compared with $V_{PUC(ref)}$, twelve pulses are produced. These pulses are the inputs of a combinational logic circuit that generates the necessary 64 minterms, which are the simplest form of Boolean expressions calculated as the product (or *AND-ed*) of all the variables, either in true or complemented form. By comparing the switching logic of seven-level CHB and PUC converters, a truth table is generated and 32 minterms are OR-gated as a group to produce the complementary switching signal pair for the PUC converter.

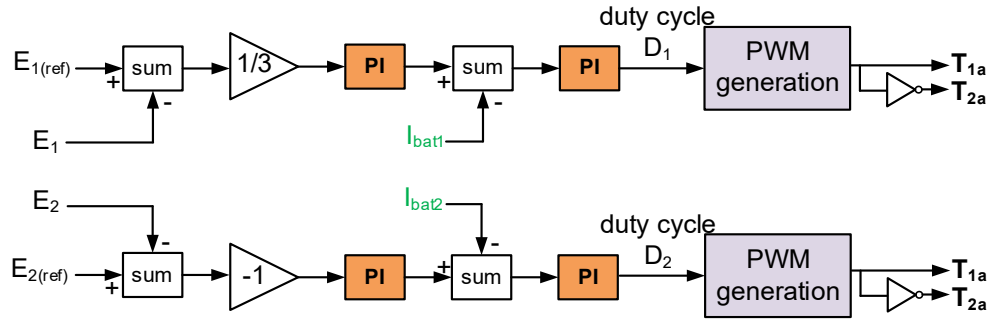


Figure 7. DC-DC converter control diagram

5. RESULTS AND DISCUSSION

To confirm the dynamic performances of the PUC-BSS controllers in both grid-tied and stand-alone modes, a simulation study is conducted with a number of case studies using the simulation parameters listed in Table 6.

Table 6. Simulation parameters

Parameter name	Parameter symbol	Value	Parameter name	Parameter symbol	Value
<i>Grid</i>			<i>PUC converter</i>		
voltage	V_G	300 V	carrier frequency	f_{sw}	5 kHz
frequency	f	50 Hz	IGBT forward voltage drop	V_f	1.037 V
Resistance	R_g	0.01 Ω	IGBT on-state resistance	R_{on}	2.146 m Ω
inductance	L_g	0.5 mH	IGBT on-state inductance	L_{on}	20 x 10 ⁻⁹ H
series L-filter	L_f	1.5 mH	DC-link 1 voltage	$E_{1(ref)}$	675 V
<i>DC-DC converter</i>			DC-link 1 voltage	$E_{2(ref)}$	225 V
switching frequency	f_{sw}	50 kHz	DC-link 1 & 2 capacitance	$C_{1,2}$	1 mF
MOSFET on-state resistance	R_{on}	0.1 Ω	DC-link 1 & 2 parasitic resistance	$R_{1,2}$	0.1 m Ω
series parasitic resistance	$R_{5,6}$	0.1 m Ω	<i>Load</i>		
			resistance	R_L	10.2 Ω
			inductance	L_L	20.12 mH
series inductance	$L_{3,4}$	13 mH	<i>Battery groups</i>		
			nominal voltage	$V_{bat1,2}$	675 V, 225 V
input capacitance	$C_{3,4}$	2000 mF	rated capacity	$C_{ap1,2}$	150 Ah
input parasitic resistance	$R_{3,4}$	0.1 m Ω	initial SOC	$SOC_{1,2}$	50 %
			response time	$t_{res1,2}$	0.1 s

The selected values of the PI controller gains for the

PUC converter control system and the DC-DC converter control system are given Appendix A. These gains were determined through an iterative trial-and-error process in the simulation environment, prioritizing a balance between fast transient response and low steady-state error while maintaining the stability of the PUC-BSS. Although time-consuming, this is a common and effective technique generally employed in simulation-based studies involving nonlinear power electronic converters.

5.1. Grid-Tied Mode

In grid-tied mode, the switches sw1 and sw2, shown in Figure 1, are turned ON and OFF, respectively, to connect the PUC-BSS to the grid. The ability of the control system to response to sudden reference changes for $I_{G-d(ref)}$ is investigated while the PUC-BSS operates in lagging power factor mode ($I_{G-q(ref)} = 40A$), consuming reactive power from the grid. The active and reactive power injected into the grid by the PUC-BSS is calculated using (4) and plotted as a function of time. During the first 0.6 s of the simulation, the batteries are commanded to discharge, and for the remaining duration, they are commanded to charge from the grid. To achieve this, a unit-step change from 30A to -30A for $I_{G-d(ref)}$ is applied at $t=0.6$ s to change the battery charging state. The instances of dynamic changes in the simulated waveforms are demonstrated in Figure 8 and Figure 9, respectively. As shown, the grid d-q axes currents track their references well after the 200ms start-up transients. It is apparent that when the state of the batteries changes, the active power injected into the grid changes its sign with a smooth transition lasting for around 10 ms. A sudden drop in the I_G signal, lasting for the same duration, also occurs. However, the grid reactive power remains constant due to the constant $I_{G-q(ref)}$. Since the grid operates in leading power factor mode, the grid current waveform leads the grid voltage waveform, delivering a constant reactive power of around -8.5 kVAR, shown on the related graph. To ensure the smooth operation of the PUC converter, its two DC-link voltages should remain at their references. As shown, both voltages remain close to their references, except for temporary transients during start-up and the set-

point change of $I_{G-d(ref)}$. The battery-related signals are illustrated in Figure 9. The battery power injections are processed with a moving average block with a frequency of 10 Hz to prevent the appearance of fast ripples. In discharging mode, the battery-1 and battery-2 inject around 9 kW and 0.2 kW, respectively into the grid. As shown, the SOC values for both batteries drop until $t=0.6$ s and begin to rise after this time.

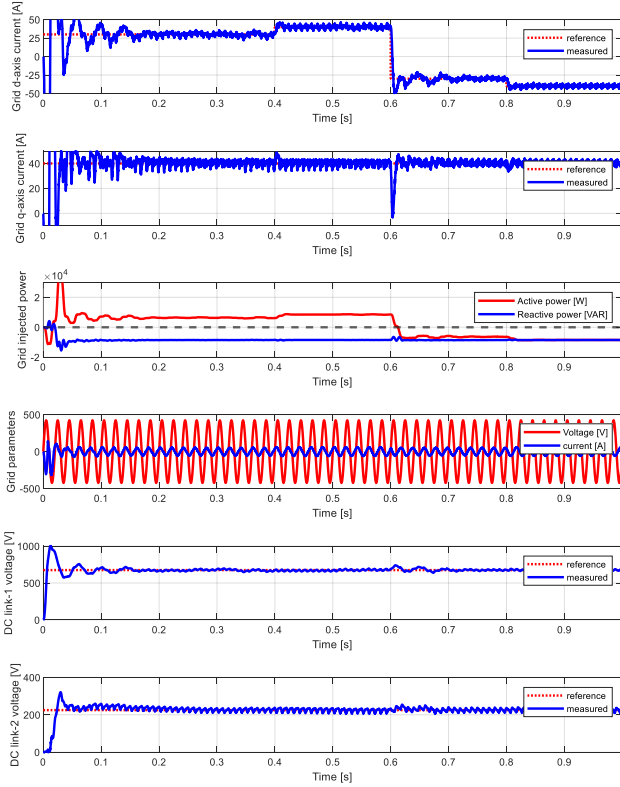


Figure 8. Simulated Waveforms of the PUC-BSS in Grid-tied Mode

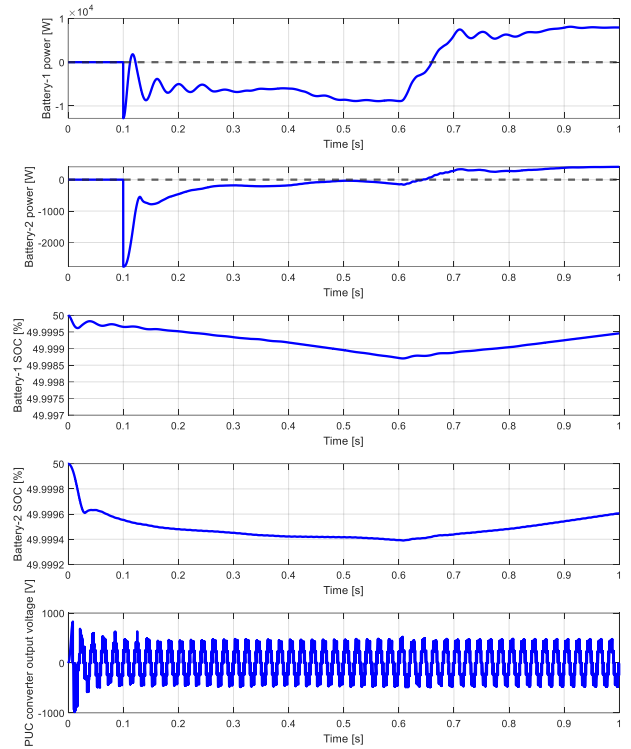


Figure 9. Simulated Waveforms of the PUC-BSS in Grid-tied Mode (continue)

At $t=0.6$ s, injected power sign changes from negative to positive, indicating a transition from discharge to charge. In charging mode, battery-1 and battery-2 absorb around 8 kW and 0.3 kW, respectively, from the grid. The difference in battery powers results from dissimilar operating battery voltages and the unsymmetrical operation of the converter. Figure 9 also shows the PUC converter output voltage as a staircase multilevel waveform. During simulations it is observed that different voltage levels are generated in accordance with the changes in set-point values. To meet the control objective, the control algorithm modifies the modulation index, which causes the voltage level count. In the second stage of the grid-tied study, the dynamic performance of the control systems for the PUC converter and the DC-DC converters is examined when the PUC-BSS functions in leading power factor mode ($I_{G-q(ref)} = -40A$), supplying VARs to the grid. The obtained signal waveforms are presented in Figure 10 and Figure 11, respectively. The grid d-axis current controls the active power injected into or absorbed from the grid. To test the performance of this controller, sudden set-point changes are applied, and the waveforms are examined. During the first 0.6 s of the simulation, a positive $I_{G-d(ref)}$ is generated to discharge the batteries.

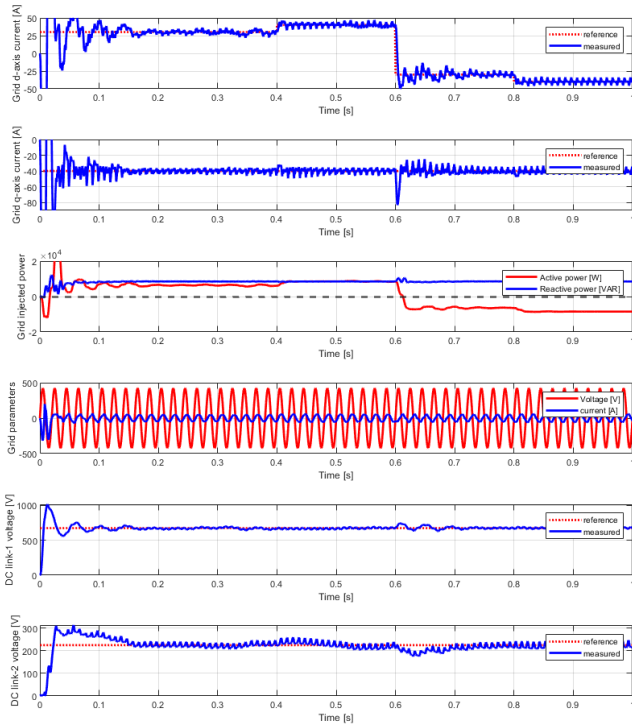


Figure 10. Simulated Waveforms of the PUC-BSS in Grid-tied Mode

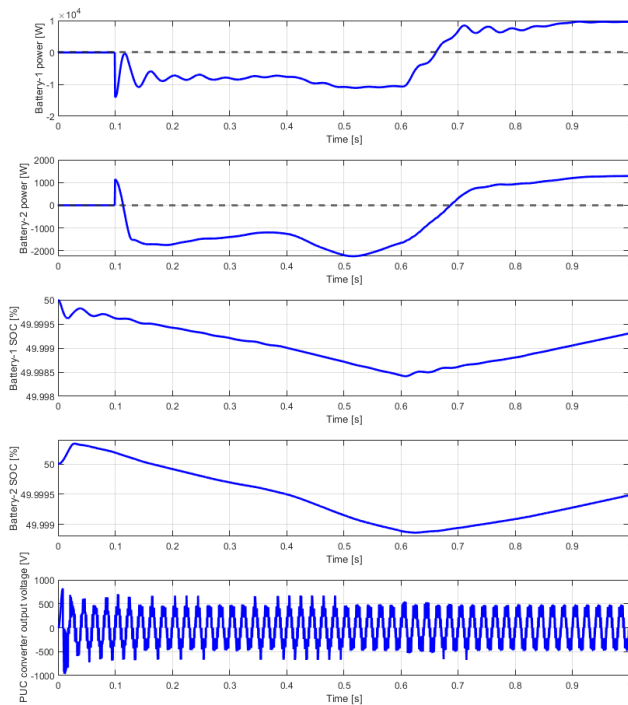


Figure 11. Simulated Waveforms of the PUC-BSS in Grid-tied Mode (continue)

After $t=0.6$ s, $I_{G-d(ref)}$ is made negative to charge the batteries. Approximately within the first 0.2 s, the start-up transients die out, and the controlled signals are able to follow their reference values with small ripple. It is thus concluded that both current controllers in the PUC-BSS control system provide sufficient dynamic performance. Moreover, the active power injected into the grid is observed to be positive during discharge and negative during charge of the batteries. The reactive power remains

positive at a constant value, since the grid operates in lagging mode. As confirmation, when the grid voltage and current waveforms are examined, the current is seen to lag behind the voltage. When the responses of the DC-link voltage controllers are examined, it is observed that both DC voltages remain at their reference values. When $I_{G-d(ref)}$ is suddenly reduced from positive to negative, a transient of approximately 100 ms is observed. On the other hand, the start-up transients lasted less than 200 ms. When examining the battery power output waveforms, it is seen that they are negative during discharge mode and positive during charge mode. The discharge-to-charge transition lasts for approximately 100 ms. When SOC of the batteries is examined, it is observed that their SOC changes according to their operating modes. It is observed that both SOC values decrease during discharging and increase during charging. In accordance with the obtained waveforms, the PUC converter output voltage dynamically changes according to the controller output signals. It is observed that the number of levels sometimes increases to seven, while at other times the converter operates at lower levels.

5.2. Stand-Alone Mode

To operate the PUC-BSS in stand-alone mode, sw1 and sw2 shown in Figure 1 are turned OFF and ON, respectively. In this way, the PUC-BSS is isolated from the grid and can feed an RL load directly. The PUC converter control algorithm shown in Figure 5 generates $V_{PUC(ref)}$ in open-loop to generate the modulation index m . The input parameters for PWM generation are set to $m = 1$ and $phase\ shift = 0$, respectively. The waveform representation of the electrical parameters is depicted in Figure 12 and Figure 13, respectively. When examining the load's current and voltage graph, it is seen that since the load type is RL, the current lags behind the voltage. On the other hand, it is shown that the load absorbs around 16 kW and 9.6 kVAR from the PUC-BSS. The initial oscillations detected while measuring the load power are due to the efforts of the DC-link voltage controllers to bring the capacitor voltages to their reference values. In this respect, it is observed that the DC-link voltages are effectively maintained at their reference values by the DC-DC converter control algorithm. When examining the battery discharge powers, it is seen that battery-1 provides approximately 17 kW of power, while battery-2 provides around 1.5 kW. The difference between total generation and consumption of the active power is due to losses in the DC-DC and PUC converters. Since both batteries are discharging while feeding the load, SOC-1 and SOC-2 simultaneously decrease from their initial values.

5.3. Harmonic Content Evaluation

The THD values of the PUC converter output voltage and current were investigated in the grid-tied and stand-

alone modes of the system. The average THD values gathered in Table 7 cover operation during battery charging and discharging under different leading/lagging power factor conditions. Because THD values vary due to transients in the controlled system variables and ripples in

Table 7. Average THD Values under Different Operating Modes for PUC-BSS

Operating mode	Batteries	PUC converter output		
			THDV	THDI
grid-tied	discharging mode $I_{G-d(ref)} = 40A$	generating Q $I_{G-q(ref)} = -40A$	33.24%	4.98%
grid-tied	discharging mode $I_{G-d(ref)} = 40A$	consuming Q $I_{G-q(ref)} = 40A$	33.91%	3.00%
grid-tied	charging mode $I_{G-d(ref)} = -40A$	generating Q $I_{G-q(ref)} = -40A$	34.34%	4.34%
grid-tied	charging mode $I_{G-d(ref)} = -40A$	consuming Q $I_{G-q(ref)} = 40A$	37.21%	4.64%
stand-alone with RL load	discharging mode	generating Q	17.64%	1.20%

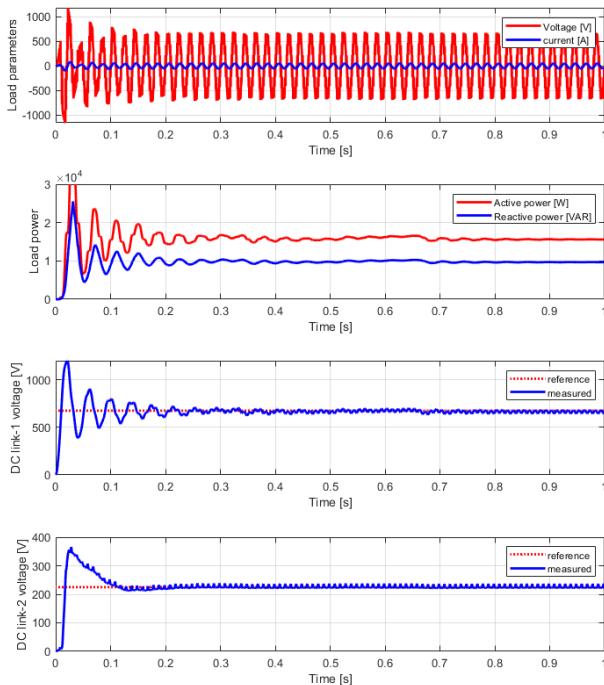


Figure 12. Simulated Waveforms of the PUC-BSS in Stand-alone Mode

the DC-link voltages of the PUC-BSS, only the last 40% of the total simulation time was used for measurement. The THD of the currents is less than 5%, which complies with the IEEE 519-2014 standard.

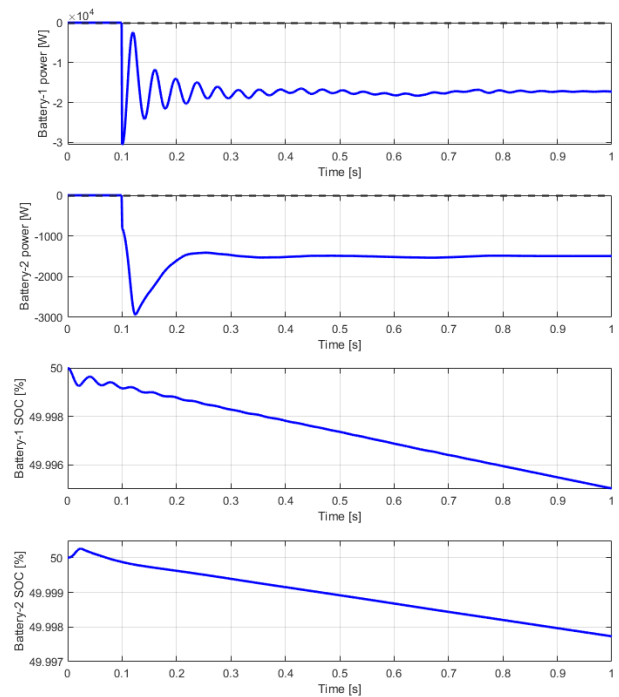


Figure 13. Simulated Waveforms of the PUC-BSS in Stand-alone Mode (continue)

6. CONCLUSIONS

In this study, a PUC-BSS was designed and verified with case studies. The PUC converter acts as an interface between the batteries and the single-phase grid to achieve charging and discharging functions in grid-tied mode. The system is also able to exchange reactive power with the grid, allowing bidirectional reactive power compensation. Although PUC converters offer many advantages, such as utilizing fewer components while achieving maximum voltage levels compared with their counterparts, they suffer from a capacitor voltage balancing issue. This is because each DC-link has a flying capacitor that must be balanced. In this study, this problem is overcome by utilizing a bidirectional DC-DC converter connected to each DC-link. This solution not only allows the batteries

to be charged and discharged in a closed-loop, but also enables regulation of the capacitor voltage of each DC-link to its reference value. The control scheme of the PUC converter and the DC-DC converter permits bidirectional active power flow between the batteries and the grid in grid-tied mode, as well as active power flow from the batteries to the load in stand-alone mode. The reactive power is also controlled bidirectionally between the grid and the PUC-BSS. The simulation results effectively verify these operations while perfectly balancing the two flying capacitor voltages. The injected grid current meets the IEEE 519–2014 standard with a simple L-filter due to the multilevel voltage output.

Declaration of Ethical Standards

The author affirms that this manuscript complies with all ethical guidelines, including proper authorship, accurate citation, transparent data reporting, and the submission of original research.

Credit Authorship Contribution Statement

The author solely undertook the conception, modeling, analysis, and preparation of this manuscript.

Declaration of Competing Interest

The author claims that there are no conflicts of interest.

Funding / Acknowledgements

No funding was received from any organization for the conduction and completion of this research.

Appendix A

PUC converter control: d-axis current controller, $K_p = 3$, $K_i = 400$, q-axis current controller, $K_p = 3$, $K_i = 20$, DC voltage controller for E_1 , $K_p = 0.1$, $K_i = 7$, DC voltage controller for E_2 , $K_p = 0.3$, $K_i = 7$, battery group-1 and group-2 current controllers, $K_p = 1$, $K_i = 50$.

References

- [1] Global Status Report for Buildings and Construction - Beyond foundations: Mainstreaming sustainable solutions to cut emissions from the buildings sector. United Nations Environment Programme (UNEP), 2024. Accessed: Sep. 30, 2025. [Online]. Available: <https://wedocs.unep.org/handle/20.500.11822/45095>.
- [2] M. Parzen, F. Neumann, A. H. Van Der Weijde, et al., "Beyond cost reduction: improving the value of energy storage in electricity systems," *Carbon Neutrality*, vol. 1, Art. no. 26, pp. 1–21, 2022. doi: 10.1007/s43979-022-00027-3.
- [3] S. Zhang, Y. Li, E. Du, et al., "Research on carbon-reduction-oriented demand response technology based on generalized nodal carbon emission flow theory," *Energies*, vol. 17, no. 18, Art. no. 4672, 2024. doi: 10.3390/en17184672.
- [4] M. H. Taabodi, T. Niknam, S. M. Sharifhosseini, H. A. Aghajari, and S. Shojaeiyan, "Electrochemical storage systems for renewable energy integration: A comprehensive review of battery technologies and grid-scale applications," *J. Power Sources*, vol. 641, Art. No. 236832, 2025. doi: 10.1016/j.jpowsour.2025.236832.
- [5] B. Yildirim, M. A. Elgendy, A. Smith, M. C. Kulan, and B. Akbal, "Modular-Multi-Port-Converter-Based Battery Energy Storage System with Integrated Battery Management Functions," *Energies*, vol. 18, no. 12, Art. no. 3142, 2025. doi: 10.3390/en18123142.
- [6] I. U. Khan and M. Jamil, "Energy Arbitrage Analysis for Market-Selection of a Battery Energy Storage System-Based Venture," *Energies*, vol. 18, no. 16, Art. no. 4245, 2025. doi: 10.3390/en18164245.
- [7] I. Thakur, "Economic viability of battery storage systems in energy-only electricity markets," in *Smart Grid and Renewable Energy Systems. ICRCE 2024. Lecture Notes in Electrical Engineering*, vol. 1238. Springer, Singapore, 2024. doi: 10.1007/978-981-97-5782-4_9.
- [8] S. Agnew and P. Dargusch, "Consumer preferences for household-level battery energy storage," *Renewable Sustainable Energy Rev.*, vol. 75, pp. 609–617, 2017. doi: 10.1016/j.rser.2016.11.030.
- [9] Z. Jin, X. Liu, W. Zhang, G. Deng, Z. Wang, N. Zhou, and J. Wang, "Operation strategies design and optimal storage capacity selection of PV-energy storage systems for residential houses under different electricity price modes," *Int. J. Green Energy*, pp. 1–20, 2025. doi: 10.1080/15435075.2025.2552487.
- [10] E. Chatterji and M. D. Bazilian, "Battery storage for resilient homes," *IEEE Access*, vol. 8, pp. 184497–184511, 2020. doi: 10.1109/ACCESS.2020.3029989.
- [11] O. Youssef and K. Al-Haddad, "A novel high energetic efficiency multilevel topology with reduced impact on supply network," in *Proc. 34th Annu. Conf. IEEE Ind. Electron., Orlando, FL, USA, Nov. 10–13, 2008*, pp. 489–494. doi: 10.1109/IECON.2008.4758002.
- [12] H. Vahedi, H. Y. Kanaan, and K. Al-Haddad, "PUC converter review: Topology, control and applications," in *Proc. 41st Annu. Conf. IEEE Industrial Electronics Society (IECON), Yokohama, Japan, 2015*, pp. 4334–4339, doi: 10.1109/IECON.2015.7392774.
- [13] H. Vahedi, A. Dehghanzadeh, K. Al-Haddad, "Static VAR compensator using packed U-cell based multilevel converter," in *Proc. IEEE 12th International Conference on Compatibility, Power Electronics and Power Engineering, Doha, Qatar, 2018*, pp. 1–5, doi: 10.1109/CPE.2018.8372576.
- [14] S. Pal, B. Avik, V. Muneer, "Open-loop capacitor voltage balancing of a nine-level packed u-cell converter," *IEEE Transactions on Industry Applications*, vol. 60, no. 4, pp. 6446–6457, 2024. doi: 10.1109/TIA.2024.3397776.
- [15] S. Abdeslem, F. Krim, A. Laib et al., "Model predictive control for single-phase active power filter using modified packed U-cell (MPUC5) converter," *Electric Power Systems Research*, vol. 180, art. no. 106139, 2020. doi: 10.1016/j.epsr.2019.106139.
- [16] M. Sleiman, H. F. Blanchette, K. Al-Haddad et al., "A new 7L-PUC multi-cells modular multilevel converter for AC-AC and AC-DC applications," in *Proc. IEEE Int. Conf. Industrial Technology (ICIT), Seville, Spain, 2015*, pp. 2514–2519, doi: 10.1109/ICIT.2015.7125468.
- [17] S. Pal and A. Bhattacharya, "Seven-level packed-U cell-based standalone PV system for water pump application," in *Proc. IEEE Int. Conf. Power Electronics, Drives and Energy Systems (PEDES), Jaipur, India, 2022*, pp. 1–6, doi: 10.1109/PEDES56012.2022.10080008.
- [18] A. Laib et al., "Novel finite-set synergetic mode predictive control of stand-alone renewable energy systems using LC-filtered nine-level packed E-cell inverter," in *Proc. 2025 IEEE Industry Applications Society Annual Meeting (IAS)*, 2025, doi: 10.1109/IAS62731.2025.11061485.
- [19] H. Iqbal, M. Tariq, M. Sarfraz, M. A. Anees, W. Alhosaini, and A. Sarwar, "Model predictive control of Packed U-Cell inverter for microgrid applications," *Energy Reports*, vol. 8, pp. 813–830, 2022, doi: 10.1016/j.egy.2022.05.188.
- [20] H. Vahedi, "5-Level Packed U-Cell (PUC5) active front-end rectifier," *IEEE Open Journal of Power Electronics*, 2025, doi: 10.1109/OJPEL.2025.3576301.
- [21] N. Mishra, B. Singh, S. K. Yadav, et al., "Power quality improvement in fifteen-level PUC converter for solar PV grid-tied applications," *IEEE Trans. Ind. Appl.*, vol. 59, no. 4, pp. 4264–4273, 2023. doi: 10.1109/TIA.2023.3260067.

- [22] R. Hariri, F. Sebaaly, K. Al-Haddad, and H. Y. Kanaan, "MPC Design and Comparative Analysis of Single-Phase 7-Level PUC and 9-Level CSC Inverters for Grid Integration of PV Panels," *Energies*, vol. 18, no. 19, Art. no. 5116, 2025. doi: 10.3390/en18195116.
- [23] T. L. Belahcene, H. Afghoul, O. Kraa, and D. E. Zábía, "Optimized control of PUC7 inverter in photovoltaic grid integration," *Electrotehnica, Electronica, Automatica (EEA)*, vol. 73, no. 3, pp. 28–38, 2025. doi: 10.46904/eea.25.73.3.1108004.
- [24] R. Hariri, F. Sebaaly, K. Al-Haddad, and H. Y. Kanaan, "Modeling and Model Predictive Control of a 7-Level Packed U-Cell Converter for Grid-Tied PV Applications," in *Proc. IECON 2024 - 50th Annu. Conf. IEEE Ind. Electron. Soc.*, Chicago, IL, USA, Oct. 2024, pp. 1–6. doi: 10.1109/IECON55916.2024.10905694.
- [25] H. Y. Hasirci and A. M. Vural, "Design and experimental verification of PUC multilevel inverter-based PMSG wind energy conversion system," *Appl. Sci.*, vol. 13, no. 24, Art. no. 13018, pp. 1–23, 2023. doi: 10.3390/app132413018.
- [26] Ananthi, K., Manoharan, S. Performance Analysis of Effective Controller for Active Power Filter using PUC5 Inverter for Improving Power Quality. *J. Electr. Eng. Technol.* 17, 2107–2121 (2022). <https://doi.org/10.1007/s42835-022-01039-w>.
- [27] S. Khettab, A. Kheldoun, and R. Bradai, "A novel Runge-Kutta-based model predictive controller for PUC7-based single-phase shunt active power filter," *Comput. Electr. Eng.*, vol. 123, Art. no. 110051, 2025. doi: 10.1016/j.compeleceng.2024.110051.
- [28] N. Decun, H. Tianqu, G. Feng, et al., "Cascaded packed U-cell STATCOM with low capacitance and its third harmonic control," in *Proc. IEEE Appl. Power Electron. Conf. Expo.*, New Orleans, LA, USA, Mar. 15–19, 2020, pp. 529–534. doi: 10.1109/APEC39645.2020.9124459.
- [29] S. Atanalian, F. Sebaaly, R. Zgheib, and K. Al-Haddad, "Z Packed U-cell modular multilevel converter for STATCOM applications," *IEEE Access*, vol. 13, pp. 78795–78800 (Page range estimated), 2025. doi: 10.1109/ACCESS.2025.3566015.
- [30] Makhamreh H, Kanzari M, Trabelsi M. Model Predictive Control of a PUC5-Based Dual-Output Electric Vehicle Battery Charger. *Sustainability*. 2023; 15(19):14483. <https://doi.org/10.3390/su151914483>.
- [31] A. M. Rauf, M. Abdel-Monem, T. Geury, et al., "A review on multilevel converters for efficient integration of battery systems in stationary applications," *Energies*, vol. 16, no. 10, Art. no. 4133, 2023. doi: 10.3390/en16104133.
- [32] F. Eroğlu, M. Kurtoglu, and A. M. Vural, "Bidirectional DC–DC converter based multilevel battery storage systems for electric vehicle and large-scale grid applications: A critical review considering different topologies, state-of-charge balancing and future trends," *IET Renewable Power Generation*, vol. 15, no. 5, pp. 915–938, 2021. doi: 10.1049/rpg2.12042.
- [33] H. A. Khalid, N. A. Al-Emadi, L. Ben-Brahim, et al., "A novel model predictive control with an integrated SOC and floating DC-link voltage balancing for 3-phase 7-level PUC converter-based MV BESS," *Int. J. Electr. Power Energy Syst.*, vol. 130, Art. no. 106895, 2021. doi: 10.1016/j.ijepes.2021.106895.
- [34] A. Azeem, M.K. Ansari, M. Tariq, et al., "Design and modeling of solar photovoltaic system using seven-level packed u-cell (PUC) multilevel inverter and zeta converter for off-grid application in India," *vol. 19, issue 2*, pp. 101–102, 2019, doi.org/10.26650/electrica.2019.18053.
- [35] X. Shunlong, M. Metry, M. Trabelsi, et al., "A model predictive control technique for utility-scale grid connected battery systems using packed U cells multilevel inverter," in *Proc. 42nd Annu. Conf. IEEE Ind. Electron. Soc.*, Florence, Italy, Oct. 23–26, 2016, pp. 5953–5958. doi: 10.1109/IECON.2016.7793712.
- [36] A. H. Azis, R. P. Eviningsih, M. R. D. Abdilla, N. S. Ramadhan, and N. A. Windarko, "Packed U-Cell Inverter with Mamdani Type Fuzzy Logic Controller to Regulate Output Voltage for Off-Grid Applications," in *Proc. 2023 Int. Electron. Symp. (IES)*, Denpasar, Indonesia, Sep. 11–13, 2023, pp. 64–69. doi: 10.1109/IES59143.2023.10242569.
- [37] T. B. J. Gemilang, M. Z. Efendi, N. A. Windarko, F. Ebrahimi, and M. R. D. Abdilla, "Voltage Regulation Optimization of a Modified Seven-Level Packed U-Cell Inverter with Mamdani Fuzzy Logic," in *Proc. 2024 Int. Electron. Symp. (IES)*, Denpasar, Indonesia, 2024, pp. 60–65. doi: 10.1109/IES63037.2024.10665812.
- [38] K. K. Malgır and E. Kılıç, "Elektrikli Araçlardan Şebekeye Enerji Verme (V2G) Sistemlerinde Packed-U Cell İnverter Tasarımı," *Kahramanmaraş Sütçü İmam Üniv. Mühendislik Bilim. Dergisi*, vol. 28, no. 3, pp. 1591–1603, 2025. doi: 10.17780/ksujes.1737399.
- [39] FF600R17ME4 700 V, 600 A dual IGBT module datasheet. (2016). Infineon Technologies. [Online]. Available: https://www.infineon.com/dgdl/Infineon-FF600R17ME4-DS-v03_00-EN.pdf?fileId=db3a304333b8a7ca0133c67bfb6d6156.
- [40] I. Baboselac, Ž. Hederić, and T. Benšić, "MatLab simulation model for dynamic mode of the Lithium-Ion batteries to power the EV," *Tehnički glasnik*, vol. 11, no. 1–2, pp. 7–13, 2017.
- [41] E. J. Lee and K. B. Lee, "Performance improvement of cascaded H-bridge multilevel inverters with modified modulation scheme," *J. Power Electron.*, vol. 21, pp. 541–552, 2021. doi: 10.1007/s43236-020-00200-w.